RSC Advances

PAPER

View Article Online
View Journal | View Issue

Cite this: *RSC Adv.*, 2014, **4**, 46427

Promotional effect of Fe on performance of Ni/SiO_2 for deoxygenation of methyl laurate as a model compound to hydrocarbons†

Xinbin Yu, Jixiang Chen* and Tianyu Ren

Received 1st August 2014
Accepted 10th September 2014

DOI: 10.1039/c4ra07932a

www.rsc.org/advances

Ni/SiO_2, Fe/SiO_2 and bimetallic $FeNi/SiO_2$ catalysts with different Fe/Ni weight ratios were prepared by incipient-wetness impregnation method for the deoxygenation of methyl laurate to hydrocarbons. It was found that a suitable amount of Fe enhanced the activity of Ni/SiO_2 for the deoxygenation of methyl laurate, and $FeNi(0.25)/SiO_2$ with a Fe/Ni weight ratio of 0.25 showed the best activity. Moreover, the addition of Fe to Ni/SiO_2 significantly promoted the hydrodeoxygenation pathway to produce more C12 hydrocarbon and suppressed the activity for C–C hydrogenolysis. The effect of Fe on the performance of Ni/SiO_2 is ascribed the formation of the NiFe alloy particles, particularly with the Fe-enriched surface at low Fe content, and the existence of oxygen vacancies in Fe oxides. A mechanism is proposed to explain the promoting effect of Fe, which involves the synergism between iron sites with strong oxophilicity and nickel sites with high ability to activate hydrogen. Besides, the effect of reaction conditions and catalyst stability were also investigated.

1 Introduction

The rapid consumption of limited reserves of fossil fuels and the subsequent negative impacts on the environment compel researchers worldwide to find alternative energy resources. In recent years, bio-fuel has been seen as a potential solution to these problems due to its renewability and intrinsic carbon neutrality.[1] Because of the high energy density and easy processing, vegetable oils are currently being widely used for production of biodiesel through transesterification.[2] However, stemming from its high oxygen content, biodiesel suffers from some detrimental problems in practice, such as poor stability, low heating value and high freezing point.[3,4] Therefore, catalytic hydrodeoxygenation of vegetable oils has attracted great attention because it can remove oxygen atoms and hydrogenate the unsaturated bonds producing diesel-like hydrocarbons (also called green diesel).[4–6]

Hydrodeoxygenation catalysts are mainly based on noble metals (Pd, Ru, *etc.*) and metal sulfides (such as MoS_2, NiMoS, and CoMoS).[7–10] Although noble metals show good performance, their high price significantly increases the operation costs. When employing the metal sulfides, the byproduct water immensely suppresses their activity.[11–13] Moreover, it is necessary to add sulfur to the feedstock to keep sulfide catalysts in a highly active state, which negatively affects the downstream processes.[14,15] It is therefore desirable to find alternative catalysts for the hydrodeoxygenation of vegetable oils. Ni-based catalysts prove to be highly active in deoxygenation of fatty acid esters.[4] However, they catalyze deoxygenation mainly through decarbonylation leading to a lower carbon yield, contrary to the concept of atom economy.[16,17] Moreover, they possess a high activity for C–C hydrogenolysis at moderate temperature, which not only further decreases the carbon yield but also consumes a large amount of hydrogen. Therefore, it is of interest to utilize the advantages of nickel catalysts and while avoiding their drawbacks.

Bimetallic catalysts have been widely applied in the petroleum industry. Incorporating a second metallic element could markedly alter the activity and selectivity of the first one due to electronic and geometric effects.[18–20] Thus, it is possible to modify the reactivity of nickel through the addition of another element. One of the potential candidates is iron. Iron catalysts have been used in the hydrogenation of carboxylic acid to aldehyde, hydrodeoxygenation of microalgal oil to green diesel, hydrodeoxygenation of guaiacol and selective reductive cleavage of inert aryl C–O bonds.[21–24] Recently, it has been reported that FeNi catalysts show special performance in the conversion of furfural to methylfuran and the hydrodeoxygenation of furfuryl alcohol, benzene alcohol and ethyl oenanthate.[25,26] In addition, iron species have redox properties as cerium and zirconium species, and cerium and zirconium species have been effectively used as supports or additives to Ni-based catalysts.[27–30] The synergistic effect between Ni and cerium and zirconium species

Tianjin Key Laboratory of Applied Catalysis Science and Technology, Department of Catalysis Science and Engineering, School of Chemical Engineering and Technology, Tianjin University, Tianjin 300072, China. E-mail: jxchen@tju.edu.cn; Fax: +86 22 87894301; Tel: +86 22 27890865

† Electronic supplementary information (ESI) available. See DOI: 10.1039/c4ra07932a

accounts for the good performance, which might also occur between Ni and Fe. Since Fe has a higher oxygen affinity than Ni,[31] iron oxide species might be available during the reaction and their oxygen vacancies can facilitate the reaction by binding and subsequently activating the oxygenates.[32–34] Although FeNi catalysts have been reported for the deoxygenation of bio-oil,[16,25,26] explicit studies remain scarce about the effect of Fe on the performance of nickel-based catalyst for the deoxygenation of fatty esters.

In the present work, we prepared silica supported Ni, Fe and FeNi catalysts with different Fe/Ni weight ratios and then investigated the effect of iron on the catalyst performance in the deoxygenation of methyl laurate as a model compound to hydrocarbons. The effects of reaction conditions as well as catalyst stability were also investigated. The result contributes to understanding the origin of the promotional effects of Fe and the design of efficient catalysts for the production of green diesel with high carbon yield.

2 Experimental

2.1 Catalyst preparation

SiO_2-supported FeNi catalysts with different Fe/Ni weight ratios (0.0625, 0.125, 0.25, 0.5 and 1) were prepared by incipient-wetness impregnation method, in which the content of nickel was kept at 8 wt%. Typically, to prepare the catalyst with Fe/Ni weight ratio of 0.25, 10 g SiO_2 (Qingdao Haiyang Chemicals Co., Ltd., 150–300 μm) was impregnated with an aqueous solution containing 1.608 g (3.980 mmol) $Fe(NO_3)_3 \cdot 9H_2O$ and 4.404 g (15.1 mmol) $Ni(NO_3)_2 \cdot 6H_2O$. Then, the sample was dried at room temperature for 48 h and subsequently at 393 K for 12 h. After that, the sample was calcined at 773 K for 4 h to produce catalyst precursor. The catalyst was generated from the precursor *via* reduction at 723 K for 1 h. For comparison, silica supported nickel and iron (8 wt%) were prepared with the procedures same to those of FeNi catalysts. The FeNi catalysts are labeled as FeNi(x)/SiO_2, where x indicates the Fe/Ni weight ratio. The properties of the fresh and spent catalysts are summarized in Table 1.

2.2 Characterization

N_2 adsorption isotherms were obtained at 77 K using Quantachrom Quadra Sorb SI. The Brunauer–Emmett–Teller (BET) was used to determine the specific surface area (S_{BET}). The pore volume and average pore size was determined by the Barrett–Joyner–Halenda (BJH) method using the desorption branch of the isotherm at a relative pressure of 0.99.

H_2 temperature-programmed reduction (H_2-TPR) was carried out in a U-tube quartz reactor (4 mm in inner diameter). The sample (50 mg) was reduced in a 10% H_2/N_2 (60 mL min^{-1}) stream at a ramping rate of 10 K min^{-1} to 1273 K. The H_2 consumption was monitored continuously by a thermal conductivity detector (TCD).

H_2 chemisorption was conducted on the same apparatus as H_2-TPR. The catalyst precursor (100 mg) was *in situ* reduced at 723 K for 1 h in H_2 (60 mL min^{-1}), and then flushed by Ar (60 mL min^{-1}) at 723 K for 1 h. After the temperature cooling to 303 K, H_2 (50 μL) pulses were injected into the Ar stream until the effluent area of consecutive pulses was constant.

X-ray diffraction (XRD) patterns were obtained on a D8 Focus powder diffractometer operated at 40 kV and 40 mA using Cu Kα radiation ($\lambda = 0.15406$ nm). Crystallite size was calculated using the Scherrer equation.

Transmission electron microscope (TEM) images were obtained on a JEM-2100F transmission electron microscope. High angle annular dark field transmission electron microscopy (HAADF-STEM) images were acquired on Tecnai G2 F20 transmission electron microscope with an FEI Titan operated at 200 kV. For TEM characterization, the power catalysts were ultrasonically dispersed in ethanol and then deposited on copper grids covered with a holey carbon film. Over 300 particles were involved to measure the metal particle size distribution. Average metal particle size was calculated by $\sum n_i d_i / \sum n_i$ (d_i: diameter of particle i, n_i: particles with d_i). The standard deviation of the mean (σ_m) was calculated by[35]

$$\sigma_m = \frac{\sum d_i^2 - n\bar{d}^2}{n^2}$$

Electron spin resonance (ESR) spectrum of reduced sample was collected by a Bruker ESP320 spectrometer at room temperature. Bruker ESP320E software and the special Bruker program were used for data analysis. The spectrum was acquired by multiple scans in order to achieve a satisfied signal to noise ratio. Before the ESR analysis, the sample was reduced at 723 K for 1 hour and then transferred to a tube in a glove box and well-sealed. Then X-band ($\upsilon = 9.78$ GHz) was recorded and the magnetic field was swept from 2000 Gauss to 4000 Gauss.

X-ray photoelectron spectroscopy (XPS) was performed on PHI5000VersaProbe instrument with Al Kα radiation (1486.6 eV) for surface elemental analysis.

Thermogravimetric analysis (TGA) was performed on Perkinelmer Pyris 1 TGA instrument with 10 mg sample at the air flow rate of 100 mL min^{-1} and temperature ramping rate of 10 K min^{-1} from room temperature to 1170 K.

2.3 Activity test

The reactivity of catalysts for the deoxygenation of methyl laurate as a model compound was tested on a continuous flow stainless-steel fixed-bed reactor (12 mm in inner diameter). In a typical run, 0.5 g catalyst was mixed with 4.0 g quartz sands with the same diameter and loaded on 1.0 g quartz sands (450–900 μm). 2.0 g quartz sands (150–300 μm) were placed on the sample to preheat the reactant. The precursor was reduced *in situ* by H_2 (>99.9%, 100 mL min^{-1}) with temperature increasing from room temperature to 723 K at a rate of 5 K min^{-1} and maintaining at 723 K for 1 h. Methyl laurate was pumped into the reactor with weight hourly space velocity (WHSV) and H_2/methyl laurate molar ratio equaling 10 h^{-1} and 25, respectively. The liquid products were identified using gas chromatograph (GC) standards and an Agilent GC6890- MS5973N and quantitatively analyzed on a SP-3420 GC equipped with a FID and a HP-5

Table 1 Properties of the silica-supported metal catalysts

Sample name	Nominal composition	BET ($m^2\ g^{-1}$)	Pore volume ($cm^3\ g^{-1}$)	Average pore size (nm)	Crystallite size[a] (nm)	d_{TEM}[b] (nm)	σ[c] (nm)	σ_m[d]	H_2 chemisorption ($\mu mol\ g_{cat.}^{-1}$)
Ni/SiO_2	8 wt% Ni	483	0.70	5.6	7.2	6.0	2.5	0.01	12.5
$FeNi(0.0625)/SiO_2$	8 wt% Ni 0.5 wt% Fe	—	—	—	7.3	—	—	—	7.2
$FeNi(0.125)/SiO_2$	8 wt% Ni 1 wt% Fe	548	0.78	5.6	7.0	—	—	—	2.8
$FeNi(0.25)/SiO_2$	8 wt% Ni 2 wt% Fe	531	0.76	5.6	6.1	5.2	2.2	0.03	—
$FeNi(0.5)/SiO_2$	8 wt% Ni 4 wt% Fe	485	0.67	5.6	6.0	4.9	2.3	0.02	—
$FeNi(1)/SiO_2$	8 wt% Ni 8 wt% Fe	454	0.58	5.6	4.1	4.9	2.0	0.01	—
Fe/SiO_2	8 wt% Fe	452	0.65	5.6	—	4.5	1.6	0.01	—
Spent Ni/SiO_2	8 wt% Ni	340	0.55	4.9	10.1	8.5	2.8	0.02	—
Spent $FeNi(0.25)/SiO_2$	8 wt% Ni 2 wt% Fe	351	0.54	4.9	6.9	6.6	1.5	0.01	—

[a] Calculated from (111) reflections using the Scherrer equation. [b] Calculated from TEM images. [c] Standard deviation. [d] The standard deviation of the mean.

capillary column (30 m × 0.33 mm × 0.5 m). Tetrahydronaphthalene was used as internal standard for quantitative analysis of liquid products. In addition, the reaction was examined to be carried out with negligible mass- and heat-transfer limitations.

Methyl laurate conversion (X) and the selectivity to product i (S_i) were defined as follows:

$$X = \frac{n_0 - n}{n_0} \times 100\%;$$

$$S_i = \frac{n_i}{n_0 - n} \times 100\%$$

where n_0 and n refer to the moles of methyl laurate in the feed and the product, respectively; n_i denotes the moles of methyl laurate converted to product i (*e.g.*, *n*-undecane, *n*-dodecane, and oxygenated intermediates).

3 Results and discussion

3.1 Catalyst characterization

3.1.1 Characterizations of precursor. Fig. 1 shows the XRD patterns of the catalyst precursors. For the Ni/SiO_2 precursor, the peaks at 37.2°, 43.3° and 62.9° are ascribed to NiO (JCPDS 71-1179). No apparent peaks attributable to iron oxide were detected for the Fe/SiO_2 precursor. In the patterns of the $FeNi/SiO_2$ precursor, the intensity of peaks due to NiO gradually decreased with increasing Fe content, indicating there was an interaction between NiO and Fe oxides promoting the dispersion of NiO. This is further reflected by the H_2-TPR results.

Fig. 2 shows the H_2-TPR profiles of catalyst precursors. The H_2-TPR profile for Ni/SiO_2 precursor exhibited a main reduction peak at about 660 K with a shoulder peak at about 735 K, which are ascribed to the reductions of NiO and Ni silicate species, respectively.[36,37] The H_2-TPR profile of Fe/SiO_2 precursor was distinctively different from those of others. The first peak at 530–780 K could be attributed to the reduction of hematite to magnetite and the second peak above 1200 K could be ascribed to the reduction of magnetite to zero valent iron.[38–40] In contrast to the Fe/SiO_2 precursor, bimetallic $FeNi/SiO_2$ precursors did not display any peaks above 800 K, implying the simultaneous reduction of iron oxide and nickel oxide.[25,41] In other words, Ni promoted the reducibility of Fe oxides, consistent with other investigations.[42] This is further confirmed by the increasing H_2 consumption with the rising Fe content in the bimetallic samples because Ni content is kept constant and Fe/SiO_2 itself cannot be completely reduced below 780 K. The promotion effect is due to easy H_2 dissociation on Ni, followed by spillover of hydrogen to iron oxide.[42] The interaction between Ni and Fe leads to the formation of a NiFe alloy, which is substantiated by the following XRD results of the reduced samples. In addition, the intensities of peaks belonging to nickel silicate species declined with the increase of Fe content, indicating that Fe species could suppress the formation of nickel silicate species possibly because certain amounts of Si–OH bonded with the Fe species instead of the Ni ones.[43]

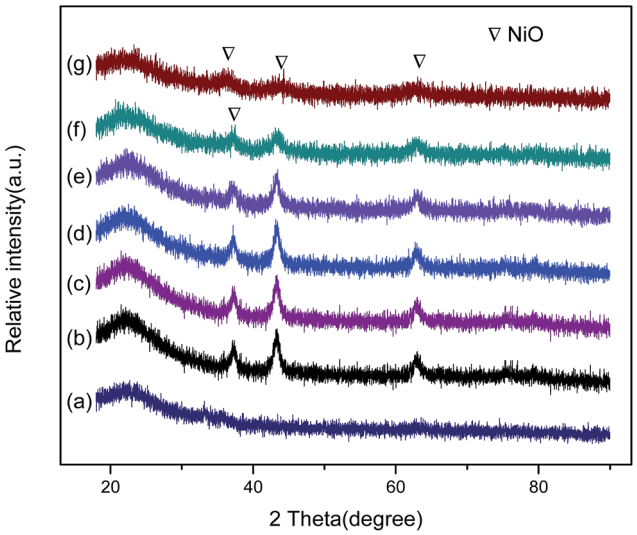

Fig. 1 XRD patterns of catalyst precursors. (a) Fe/SiO_2, (b) Ni/SiO_2, and bimetallic $FeNi/SiO_2$ with Fe/Ni weight ratios of (c) 0.0625 : 1, (d) 0.125 : 1, (e) 0.25 : 1, (f) 0.5 : 1, and (g) 1 : 1.

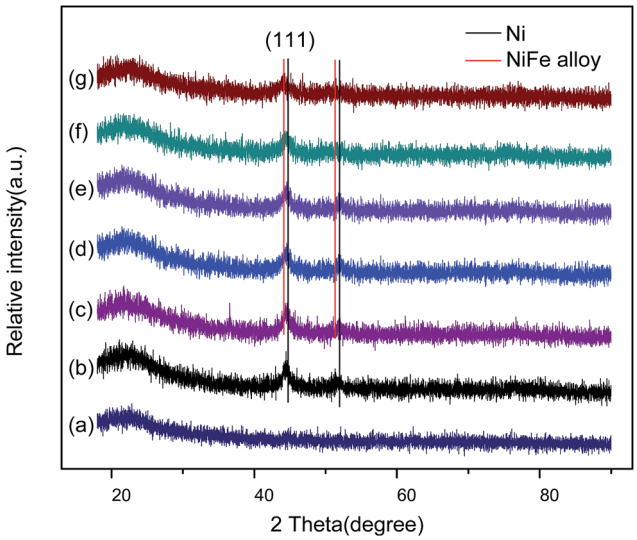

Fig. 3 XRD patterns of reduced samples. (a) Fe/SiO_2, (b) Ni/SiO_2, and bimetallic $FeNi/SiO_2$ with Fe/Ni weight ratios of (c) 0.0625 : 1, (d) 0.125 : 1, (e) 0.25 : 1, (f) 0.5 : 1, and (g) 1 : 1.

3.1.2 Characterizations of catalysts. The XRD patterns of reduced catalysts are presented in Fig. 3. For Ni/SiO_2, two diffraction peaks centered at $2\theta = 44.5°$ and 51.8° correspond to (111) and (200) reflections of the fcc Ni metal phase (JCPDS 01-070-1849). However, for bimetallic catalysts, the peak corresponding to (111) gradually shifted to low angle with the increase of Fe content, in accordance with other reports.[16,36,44] This is ascribed to the formation of NiFe alloy with fcc structure whose peak is located at $2\theta = 43.5°$.[45,46] The more the Fe atoms existed in the alloy, the more obvious the shift was.[16,47] No peaks due to monometallic Fe were detected for Fe/SiO_2, which is ascribed to the high dispersion of Fe as well as the incomplete reduction of Fe oxides at 723 K. The average diameters of Ni or NiFe alloy crystallites were calculated using Scherrer equation based on the (111) reflections (Table 1). The crystallite size decreased with increasing Fe content, indicating that Fe promoted the dispersion of Ni. This is further verified by the TEM results.

Fig. 4 shows the TEM images and metal particle size distributions of some reduced catalysts. The average metal particle sizes in Ni/SiO_2 and Fe/SiO_2 were 6.0 and 4.5 nm, respectively. The average metal particle sizes in bimetallic $FeNi/SiO_2$ were smaller than that of Ni/SiO_2. As indicated by standard deviation (Table 1), the particle diameter distributions for all catalysts were wide. However, the standard deviation of the mean (σ_m) was very small, indicating that the observed distribution closely approached the true population.[35] Moreover, it is generally acknowledged that the particles grow large with the increasing metal loading, which was, however, not the case of the present samples. In all, Fe promoted the dispersion of Ni as reflected by both XRD and TEM results.

From the thermodynamic viewpoint,[48] it is expected that the more stable FeNi clusters will have the nickel inside,[49] since the cohesive energy of bulk nickel is slightly greater than for bulk iron (428 *vs.* 413 kJ mol^{-1}),[50] which have been reported by many references.[16,41,42,45,51] To further verify the formation of NiFe alloy and the Fe and Ni concentration distribution in the bimetallic catalysts, $FeNi(0.5)/SiO_2$ was characterized by HRTEM and STEM-EDS (see Fig. 5 and 6). For $FeNi(0.5)/SiO_2$, the lattice spacing of the fringes was 0.205 nm, which can be attributed to the (111) plane of fcc NiFe alloy (Fig. 5). Elemental mapping analysis for $FeNi(0.5)/SiO_2$ sample based on HAADF-STEM-EDS (Fig. 6(B)) displays a more uniform distribution of Fe than that of Ni. The Fe and Ni distributions within an individual alloy particle were indicated by STEM-EDS line-scanning spectra (Fig. 6(D), (F) and (H)), which suggested that the Fe and Ni

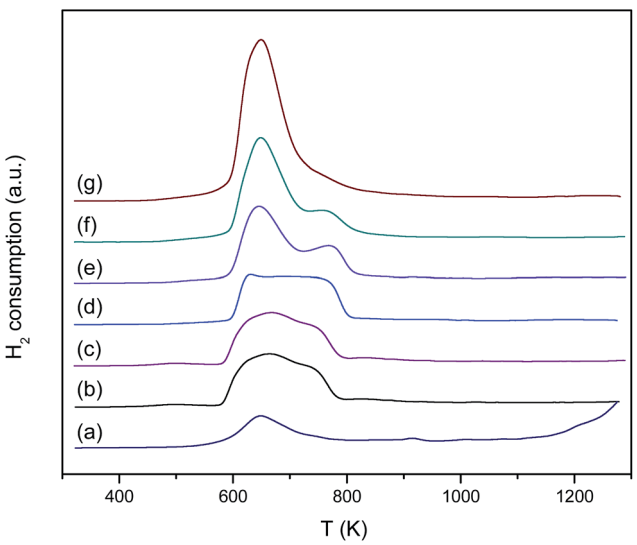

Fig. 2 H_2-TPR profiles of catalyst precursors. (a) Fe/SiO_2, (b) Ni/SiO_2, and bimetallic $FeNi/SiO_2$ with Fe/Ni weight ratios of (c) 0.0625 : 1, (d) 0.125 : 1, (e) 0.25 : 1, (f) 0.5 : 1, and (g) 1 : 1.

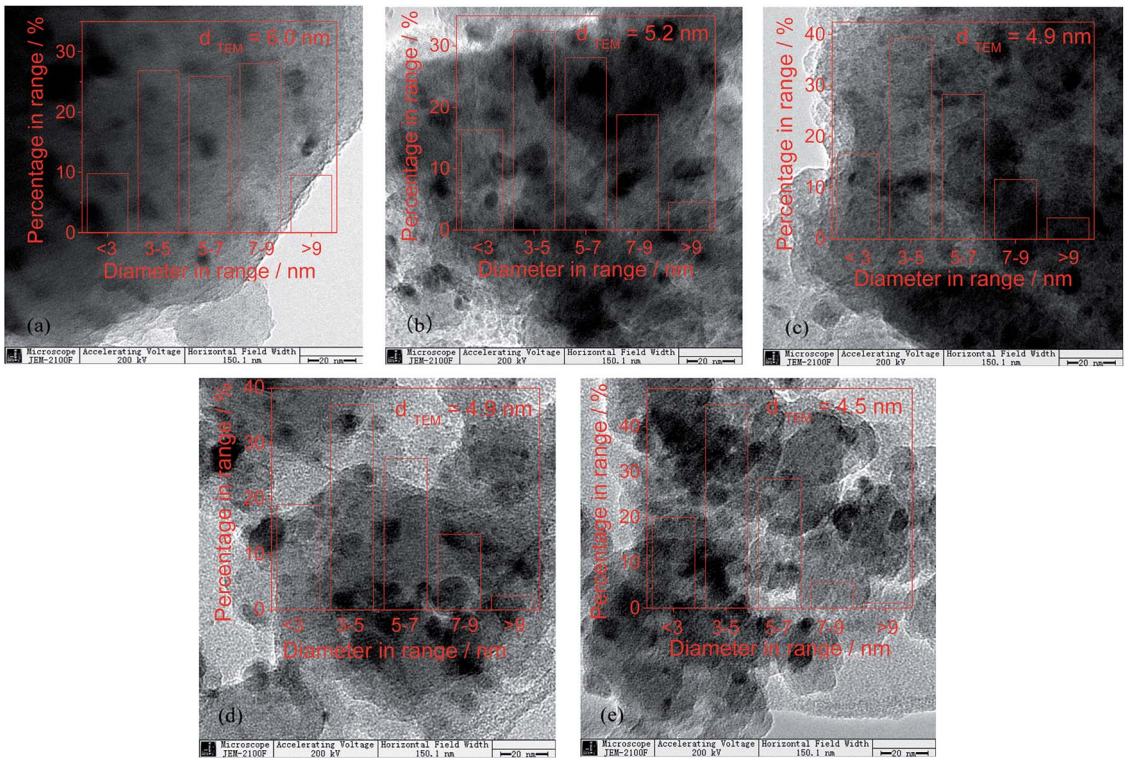

Fig. 4 TEM images of reduced samples. (a) Ni/SiO_2, bimetallic FeNi/SiO_2 with Fe/Ni weight ratios of (b) 0.25 : 1, (c) 0.5 : 1, (d) 1 : 1 and (e) Fe/SiO_2.

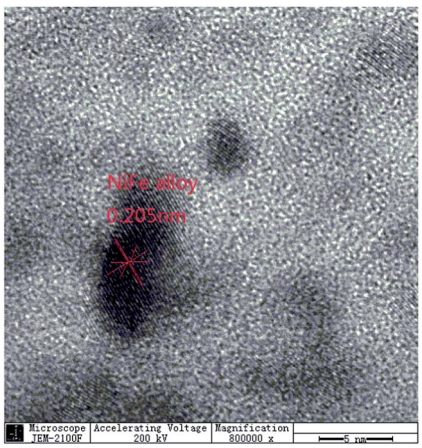

Fig. 5 HRTEM image of FeNi/SiO_2 with Fe/Ni weight ratio of 0.5 : 1.

distributions in the bimetallic particles varied in terms of the Fe content. For the FeNi(0.25)/SiO_2 sample, the M shape of the line-scanning spectrum (0–15 nm) for Fe implied that Fe was enriched on the particle surface. However, with increasing Fe content (*i.e.*, for the FeNi(0.5)/SiO_2 and FeNi(1)/SiO_2 samples), both Ni and Fe tended to be homogenous distribution in the single alloy particle. That is, Fe might be enriched on the bimetallic particles at low Fe contents. This is also supported by the following results, *i.e.*, sharp decreases of the H_2 chemisorption (Table 1) and the C–C bond hydrogenolysis and decarbonylation ability of Ni (Fig. 7) due to the addition of tiny amount of Fe.

To obtain information about the catalyst surface, FeNi(0.5)/SiO_2 was also characterized by XPS. The surface Fe/Ni atomic ratio determined from XPS spectrum was about 2.5, *i.e.*, about five times the nominal bulk atomic Fe/Ni ratio (0.5). Thus, Fe species were rich on the catalyst surface.

H_2 uptakes of the reduced catalysts are displayed in Table 1. H_2 uptake of Ni/SiO_2 was 12.5 μmol g^{-1}. Interestingly, although the addition of Fe to Ni/SiO_2 promoted the metal dispersion as indicated by XRD and TEM results, it indeed reduced the H_2 uptake. Moreover, with the increase in Fe content, H_2 uptakes drastically decreased and there was no apparent H_2 chemisorption for FeNi(x)/SiO_2 ($x > 0.125$). That is, the addition of Fe blocked the H_2 adsorption on Ni sites. This is possibly due to coverage of Ni sites with Fe species on the Fe-enriched surface,[51] because Fe has a lower activity for H_2 adsorption and activation. Similar effects of Fe have been widely reported.[44,47,52,53]

The BET surface area and pore structure of reduced catalysts are also listed in Table 1. The BET surface area decreased with the increase of Fe content ($x \geq 0.125$). Compared to the Ni/SiO_2 sample, FeNi (0.125–0.5)/SiO_2 had a larger surface area, which indicated that a suitable amount of Fe could improve the BET surface of Ni/SiO_2.

3.2 Catalytic reactivity

A control experiment filling the reactor tube with SiO_2 quartz sand was conducted under the same reaction conditions which exhibited scarce conversion of methyl laurate. The main liquid products in the deoxygenation of methyl laurate on monometallic and bimetallic catalysts were *n*-undecane (C11), *n*-

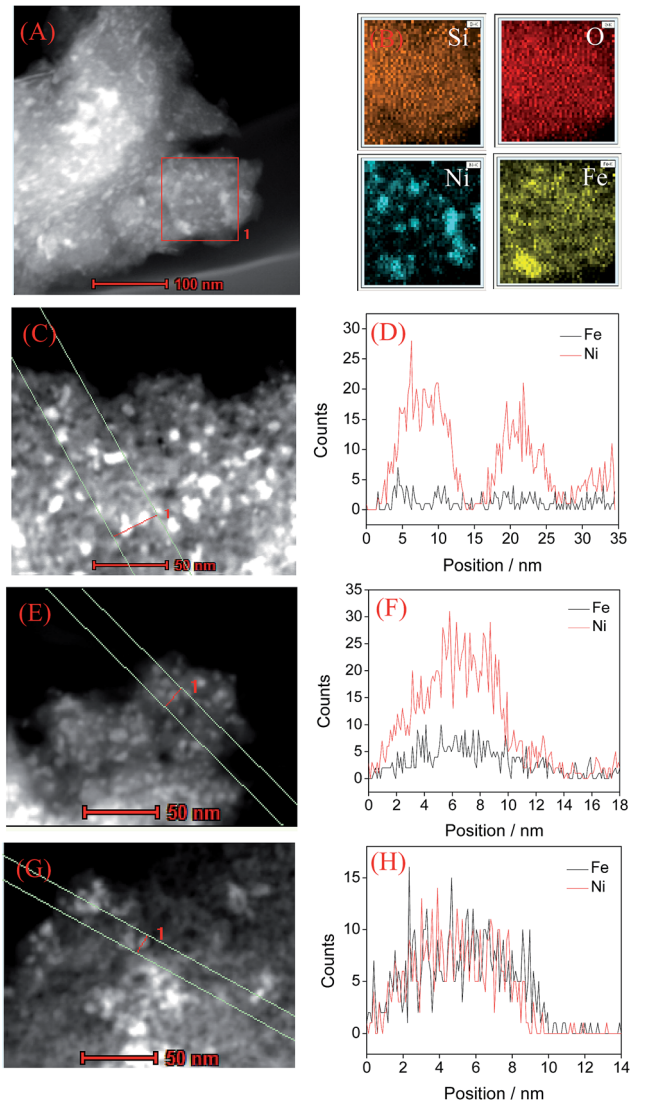

Fig. 6 STEM images and structural characterizations for FeNi/SiO_2 with Fe/Ni weight ratios of (A), (E) 0.5 : 1, (C) 0.25 : 1 and (G) 1 : 1. (B): EDS mapping of the square area in (A); (D), (F) and (H): EDS line-scanning spectra for Fe–K (black) and Ni–K (red) along the red line in (C), (E) and (G), respectively.

dodecane (C12), cracked hydrocarbons (C7–C10, including *n*-heptane, *n*-octane, *n*-nonane and *n*-decane), and oxygenated intermediates (dodecanol, dodecanal, dodecoic acid and lauryl laurate). Among the oxygenated intermediates, dodecanol was dominating (except the case of Fe/SiO_2, in which both dodecanol and lauryl laurate were major products). In addition, there were very low amounts of isomerized hydrocarbons, alkenes and cyclododecane. The reaction network is proposed in Scheme 1 based on previous studies.[54,55]

3.2.1 Effect of Fe/Ni ratio. Fig. 7 displays the effect of the Fe/Ni weight ratios on the catalyst reactivity. Fig. 7(a) indicated that Fe/SiO_2 had a lower activity for deoxygenation of methyl laurate than Ni/SiO_2. However, Fe presented a promoting effect on the activity of Ni/SiO_2. The FeNi/SiO_2 catalysts with Fe/Ni ratio ≤0.5 gave a higher conversion than Ni/SiO_2. As the Fe

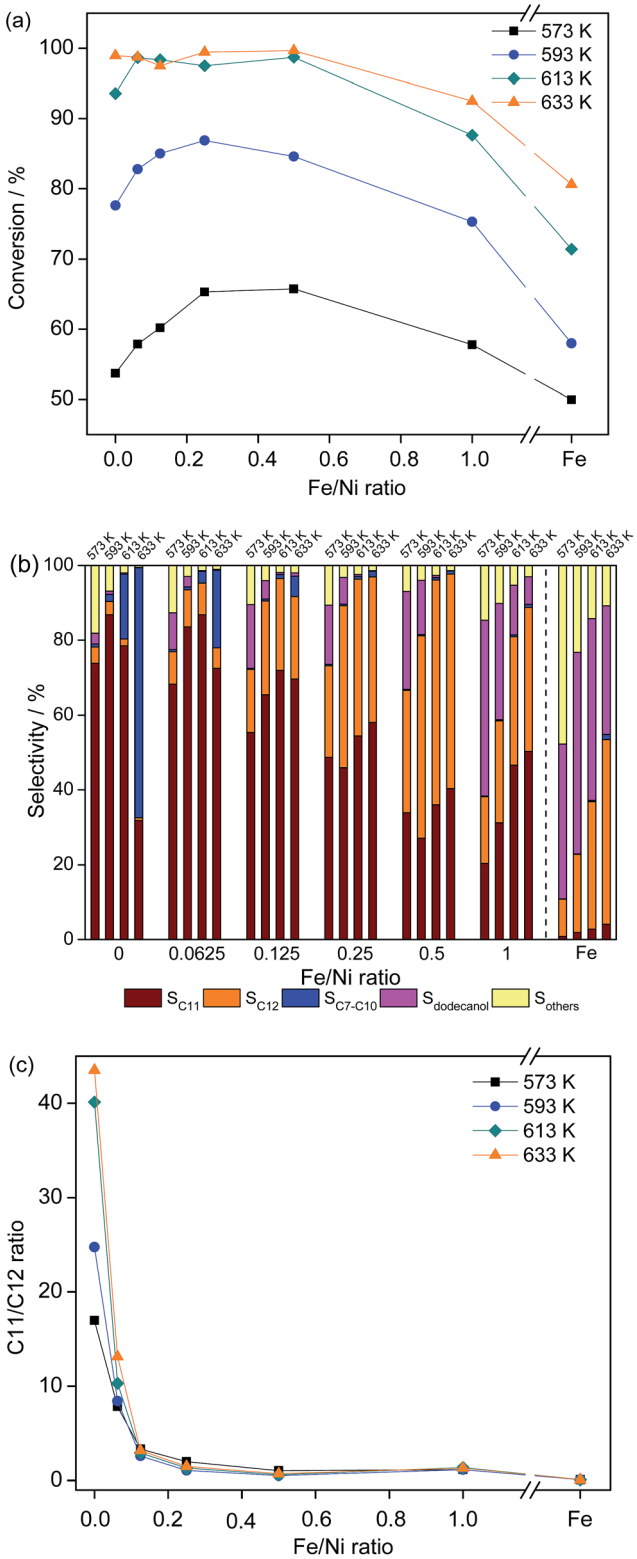

Fig. 7 Performance of deoxygenation of methyl laurate as a function of temperature and Fe/Ni weight ratios. Other products include dodecanal, dodecoic acid, cyclododecane and lauryl laurate. Reaction conditions: 3 MPa H_2, WHSV of 10 h^{-1}, H_2/methyl laurate molar ratio of 25.

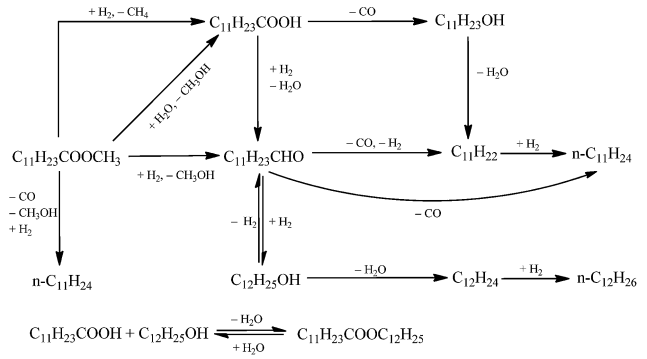

Scheme 1 Reaction network of deoxygenation of methyl laurate.

content increased, the conversion exhibited a slight volcano curve and reached the maximum at the Fe/Ni ratio of 0.25. With the Fe/Ni ratio increasing from 0 to 0.25, the conversion increased from 53.7% to 65% at 573 K and from 78% to 87% at 593 K. However, the conversion decreased as the Fe/Ni ratio exceeded 0.25. Clearly, suitable Fe contents were needed for enhancing the activity of Ni/SiO_2. Furthermore, the addition of Fe to Ni/SiO_2 remarkably changed the product distribution. As depicted in the Fig. 7(b) and (c), the main hydrogenated products on Ni/SiO_2 and Fe/SiO_2 were C11 and C12 hydrocarbons, respectively. That is, the deoxygenation of methyl laurate on Ni/SiO_2 and Fe/SiO_2 mainly occurred *via* decarbonylation and HDO pathways, respectively. The addition of Fe to Ni/SiO_2 reduced the selectivity to C11(S_{C11}) but enhanced the selectivity to C12(S_{C12}). This is more obviously reflected by the molar ratio between C11 and C12 hydrocarbons (C11/C12 ratio), which represents the selectivity between decarbonylation and HDO pathways. As shown in (Fig. 7(c)), the C11/C12 ratio sharply decreased as the Fe/Ni ratio increased and then almost did not change when the Fe/Ni ratio was larger than 0.25. Besides, the addition of Fe to Ni/SiO_2 restrained the formation of cracked products (see Fig. 7(b)). The larger the Fe/Ni ratio was, the less the cracked products formed, which was more obvious at high temperature. At 633 K, for instance, the selectivity to cracked products (C7–C10) was 67% on Ni/SiO_2, while it was only 2% on $FeNi(0.25)/SiO_2$. The reduction of the selectivity to cracked products is very significant in practice because of enhancing the carbon yield as well as reducing H_2 consumption. In short, Fe made a significant effect on the performance of Ni/SiO_2. This is mainly related to the formation of NiFe alloy.

As indicated in Section 3.1.2, Fe was enriched on the surface of the NiFe alloy particles, especially at low Fe contents, and also restrained the H_2 chemisorption. Moreover, Fe/SiO_2 showed a lower activity than Ni/SiO_2 for deoxygenation of methyl laurate. Surprisingly, the activity of Ni/SiO_2 was enhanced when a suitable amount of Fe (Fe/Ni weight ratio $\leq$0.5) was added. We suggest that this promoting effect results from the synergism between Ni and Fe species.

It is known that Ni has higher H_2 adsorption and activation abilities but a weaker oxygen affinity than Fe.[16,31] Based on the DFT calculations, it has been found that the metal–oxygen affinity follows the sequence of Fe > NiFe alloy > Ni,[16] and that the eta-2-(C,O) species is more stable on NiFe alloy than on monometallic Ni.[25] From ESR spectra (Fig. S2†), we also found the existence of Fe–O–Fe species with ferri-, ferro-, and/or antiferromagnetic behavior on $FeNi(0.25)/SiO_2$,[56] in agreement with the other observations.[16,57–59] The oxygen vacancies on the iron oxide can bind oxygen atom in the C=O group *via* the donation of the lone pair of electrons and subsequently the C=O bond is activated.[21,32–34,60,61] The strong oxygen affinity of Fe and the role of oxygen vacancies in Fe oxide can account for the dominating HDO pathway on Fe/SiO_2 because the activated C=O group *via* O adsorption on Fe site can be readily hydrogenated to dodecanol and subsequently dehydrated/hydrogenated to produce C12 hydrocarbon. For bimetallic $FeNi/SiO_2$, the oxygen in C=O group is more preferentially adsorbed on Fe sites (either metallic Fe atoms or Fe oxides) than the Ni ones. The Ni and Fe sites could be synergetic in promoting the conversion of methyl laurate. In other words, H_2 is easily activated and dissociated on Ni sites and spills over to the neighbouring Fe sites that adsorb oxygen atom of C=O group of methyl laurate, where the hydrogenation takes place leading to the HDO product. The process is proposed in Scheme 2. As a result, the synergism between Ni and Fe sites promotes not only the conversion of methyl laurate but also the HDO pathway (*i.e.*, formation of C12). Further, an interesting phenomenon is noteworthy as shown in Fig. 7(b), *i.e.*, the selectivity to dodecanol ($S_{dodecanol}$) increased with the Fe content. This is undoubtedly attributable to the promoting role of Fe for the HDO pathway since dodecanol is an intermediate in the HDO pathway. The promotional effect on the HDO pathway due to the increase in oxygen affinity of metal sites has also been found in the metal phosphide and sulfide catalysts.[55,62] As indicated by

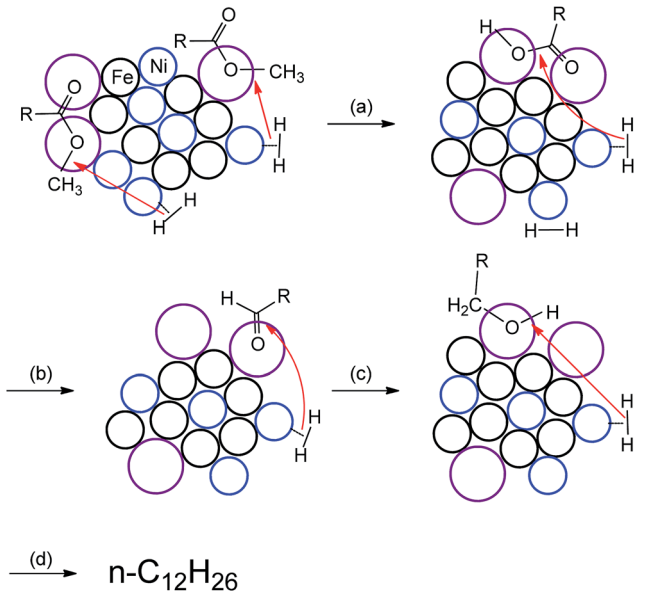

Scheme 2 Possible reaction mechanism for the HDO pathway in the deoxygenation of methyl laurate on $FeNi/SiO_2$, (a) hydrogenolysis to dodecoic acid; (b) reduction to dodecanal; (c) reduction to dodecanol; (d) dehydration and then hydrogenation to n-$C_{12}H_{26}$; R denotes n-$C_{11}H_{23}$.

Fig. 7(a), to reach maximum synergism for the catalyst activity, the Fe/Ni ratio should be 0.25. When the Fe/Ni ratio exceeds 0.25, the excess Fe covers the Ni sites, leading to a decrease in the hydrogen-activating ability and subsequently the activity,[63] such as the case for FeNi(1)/SiO_2.

As mentioned above, the selectivity to cracked hydrocarbons was remarkably reduced by the addition of Fe to Ni/SiO_2. This is also related to the formation of NiFe alloy and the Fe rich surface of NiFe alloy particles. It is well accepted that the C–C hydrogenolysis requires consecutive Ni sites.[64] However, the formation of NiFe alloy with Fe enriched surface leads to the disruption of the adjacent Ni atoms, thus the C–C hydrogenolysis was suppressed. Similarly, Cu has also been found decreasing the C–C hydrogenolysis activity of Ni due to geometry effect.[20,65]

3.2.2 Effect of reaction conditions. Fig. 7 also shows the effect of temperature on the performance of different catalysts. For each catalyst, increasing temperature promoted the conversion of methyl laurate due to the increased reaction rate. As the temperature rose from 573 to 633 K, the total selectivity to C11 and C12 firstly increased and then decreased for Ni/SiO_2 and FeNi(x)/SiO_2 (x = 0.0625 and 0.125), while it always increased for FeNi(x)/SiO_2(x = 0.25–1). At high temperature, the decreased selectivity to C11 and C12 is ascribed to the promoted cracking. It is noteworthy that the effect of temperature on the selectivity to cracked products is more pronounced for Ni/SiO_2 in comparison with FeNi(x)/SiO_2. This further confirms that the formation of NiFe alloy is vital for the performance of FeNi(x)/SiO_2. In addition, $S_{dodecanol}$ decreased with the rise of temperature because high temperature favored the dehydration of dodecanol. As dodecanol was detected as the main intermediate on FeNi(x)/SiO_2($x \geq 0.125$), its dehydration might be a rate-determining step during the deoxygenation of methyl laurate.

Since FeNi(0.25)/SiO_2 exhibited a good deoxygenation performance, the effects of WHSV and H_2 pressure on its performance were investigated.

Fig. 8 displays the effect of WHSV of methyl laurate on the performance of FeNi(0.25)/SiO_2. As the WHSV rose from 3 to 20 h^{-1}, the conversion and the selectivity to C11 (S_{C11}) decreased from 98% to 43% and from 71% to 35%, respectively, while the selectivity to C12 (S_{C12}) did not change. The C11/C12 ratio tended to decrease, indicating that HDO pathway was promoted by increasing WHSV. This is more obviously reflected by the C11/C12* ratio (C12* includes C12 and dodecanol) as dodecanol is an intermediate in the HDO pathway. In addition, the selectivity to dodecanol ($S_{dodecanol}$) increased from 0 to 30%. The increase of WHSV corresponds to the decrease of the contact time of reactants on the active sites, which reduces the conversion of methyl laurate as well as intermediates (for instance, dodecanol). The result also indicates that the dehydration of dodecanol may be the rate-determining step during the deoxygenation of methyl laurate.

The effect of H_2 pressure on the performance of FeNi(0.25)/SiO_2 is shown in Fig. 9. With the pressure increasing from 2 to 5 MPa, the conversion and the selectivity to C11 and C12 tended to slightly decrease, while the selectivity to dodecanol increased from 10% to 22%. The C11/C12 ratio increased with the rise of pressure. This seems to indicate that the increase of H_2 pressure favors the decarbonylation pathway. In fact, since dodecanol was an intermediate during the HDO pathway, the C11/C12* might be more reasonable to reflect the selectivity between the decarbonylation and HDO pathways, and it gradually decreased with the increasing pressure. This suggests that high pressure favors the HDO pathway, which is probably due to the increased hydrogen concentration on the catalyst surface.

3.2.3 Catalyst stability. Stability is an important property of catalyst. Fig. 10 shows the conversion, total selectivity to C11 and C12 ($S_{C11+C12}$) and C11/C12 ratio on Ni/SiO_2 and FeNi(0.25)/SiO_2 as a function of time. For FeNi(0.25)/SiO_2, the initial conversion was nearly 100% and decreased to 95% at the 61st hour. For Ni/SiO_2, the conversion was about 94% at the beginning and decreased to 87% at the 61st hour. Clearly, both Ni/SiO_2 and FeNi(0.25)/SiO_2 deactivated but they had similar stability during 61 hours. $S_{C11+C12}$ on FeNi(0.25)/SiO_2 maintained above 98% during 61 hours, much larger than that

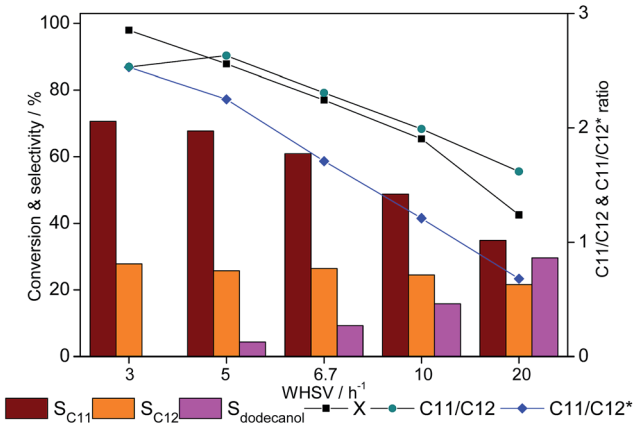

Fig. 8 Deoxygenation of methyl laurate on FeNi/SiO_2 with Fe/Ni weight ratio of 0.25 : 1 as a function of WHSV. Reaction conditions: 573 K, 3 MPa H_2, H_2/methyl laurate molar ratio of 25.

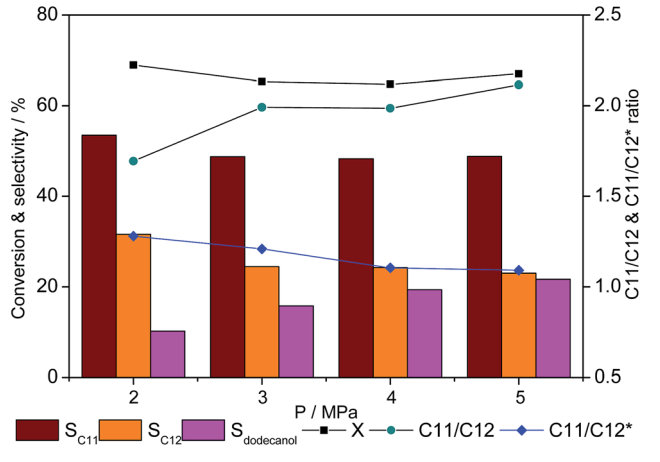

Fig. 9 Deoxygenation of methyl laurate on FeNi/SiO_2 with Fe/Ni weight ratio of 0.25 : 1 as a function of H_2 pressure. Reaction conditions: 573 K, WHSV of 10 h^{-1}, H_2/methyl laurate molar ratio of 25.

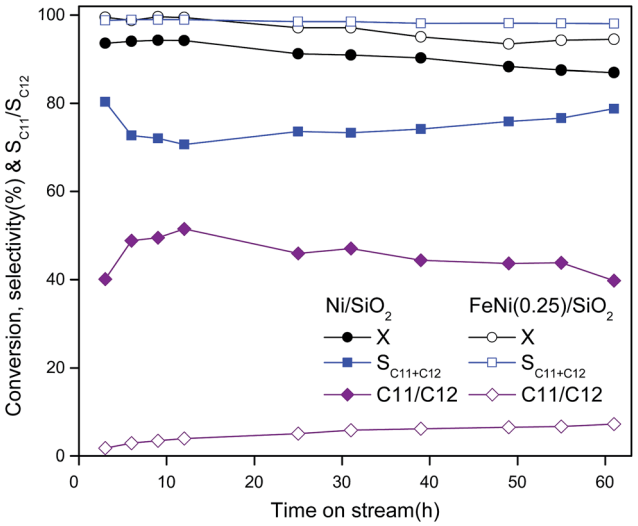

Fig. 10 Conversion, selectivity to C11 and C12 and C11/C12 ratio on Ni/SiO_2 and $FeNi/SiO_2$ with Fe/Ni weight ratio of 0.25 : 1 as the function of time. Reaction conditions: 613 K, 3 MPa H_2, WHSV of 10 h^{-1}, H_2/methyl laurate molar ratio of 25.

(70–80%) on Ni/SiO_2. This is due to the higher selectivity to cracked products on Ni/SiO_2 (see Fig. S2†). In addition, with the extension of time, the C11/C12 ratio steadily increased from 1.8 to 7.8 on $FeNi(0.25)/SiO_2$, while it fluctuated between 40 and 51 on Ni/SiO_2. On the whole, compared with Ni/SiO_2, $FeNi(0.25)/SiO_2$ gave a higher activity and selectivity to target hydrocarbons as well as similar stability.

To obtain the properties of catalyst after reaction, the spent catalysts were characterized. From the metal particle sizes before and after reaction for 61 h (see Table 1, Fig. S3 and S4†), it was found that the sintering of metal particles on Ni/SiO_2 was more serious than that on $FeNi(0.25)/SiO_2$. That is, the addition of Fe inhibited the growth of Ni particles. TGA (Fig. S5†) showed that a little more amount of coke formed on $FeNi(0.25)/SiO_2$(8.9%) than on Ni/SiO_2(6.3%). We speculate that the $FeNi(0.25)/SiO_2$ deactivation is mainly attributed to coke, while the Ni/SiO_2 deactivation is also derived from the sintering of Ni particles apart from coke. The BET surface areas of spent catalysts were displayed in Table 1. Compared to that of the fresh samples, spent catalysts had a much lower BET surface area, which could mainly be ascribed to the formation of coke.

4 Conclusions

In the present work, we provided an approach to improving activity and tuning the production distribution by addition of Fe to Ni/SiO_2, and proposed that the NiFe alloy particles, especially with Fe-enriched surface at low Fe loading and the oxygen vacancy in FeO_x contributed to the special performance of $FeNi/SiO_2$. The geometric effect of Fe significantly restrained the C–C hydrogenolysis activity of Ni/SiO_2. On the surface of NiFe alloy particles, the Ni and Fe species, which respectively possessed a high ability to activate hydrogen and a strong oxygen affinity, were synergetic in promoting the conversion of methyl laurate through HDO pathway. Among the catalysts tested, $FeNi(0.25)/SiO_2$ exhibited the best performance. We also investigated the effect of reaction conditions on the catalysts performance. What is worth mentioning here is that as the temperature increased, the cracking and decarbonylation pathway were promoted more remarkably on Ni/SiO_2 than on $FeNi/SiO_2$. This further indicates that there is an essential difference in structure and performance between Ni/SiO_2 and $FeNi/SiO_2$. On the whole, the increase of temperature and the deceases of WHSV and H_2 pressure enhanced the catalyst activity while promoted the decarbonylation pathway rather than the HDO one. Under the condition of 613 K, 3 MPa, WHSV of 10 h^{-1} and H_2/methyl laurate molar ratio of 25, $FeNi(0.25)/SiO_2$ had comparable stability to Ni/SiO_2 during 61 h. After reaction for 61 h, $FeNi(0.25)/SiO_2$ gave the conversion of 94% and the selectivity to C11 and C12 of 98%, much higher than those on Ni/SiO_2. Our finding may provide important information for the rational design of Ni-based catalysts for the production of green diesel with high carbon yield.

Acknowledgements

The authors gratefully acknowledge the supports from the National Natural Science Foundation of China (no. 21176177), the Natural Science Foundation of Tianjin (no. 12JCYBJC132 00) and the Program of Introducing Talents to the University Disciplines (B06006).

Notes and references

1 A. Corma, G. W. Huber, L. Sauvanaud and P. O'connor, *J. Catal.*, 2007, **247**, 307–327.
2 S. Lestari, P. Mäki-Arvela, J. Beltramini, G. Q. Lu and D. Y. Murzin, *ChemSusChem*, 2009, **2**, 1109–1119.
3 E. Santillan-Jimenez, T. Morgan, J. Lacny, S. Mohapatra and M. Crocker, *Fuel*, 2013, **103**, 1010–1017.
4 H. Zuo, Q. Liu, T. Wang, L. Ma, Q. Zhang and Q. Zhang, *Energy Fuels*, 2012, **26**, 3747–3755.
5 K. Murata, Y. Liu, M. Inaba and I. Takahara, *Energy Fuels*, 2010, **24**, 2404–2409.
6 I. Simakova, O. Simakova, P. Mäki-Arvela, A. Simakov, M. Estrada and D. Y. Murzin, *Appl. Catal., A*, 2009, **355**, 100–108.
7 L. He, C. Wu, H. Cheng, Y. Yu and F. Zhao, *Catal. Sci. Technol.*, 2012, **2**, 1328–1331.
8 M. Chiappero, P. T. M. Do, S. Crossley, L. L. Lobban and D. E. Resasco, *Fuel*, 2011, **90**, 1155–1165.
9 B. Veriansyah, J. Y. Han, S. K. Kim, S. A. Hong, Y. J. Kim, J. S. Lim, Y. W. Shu, S. G. Oh and J. Kim, *Fuel*, 2012, **94**, 578–585.
10 E. Furimsky, *Catal. Today*, 2013, **217**, 13–56.
11 E. Laurent and B. Delmon, *J. Catal.*, 1994, **146**, 281–291.
12 Y. Yoshimura, T. Sato, H. Shimada, N. Matsubayashi and A. Nishijima, *Appl. Catal.*, 1991, **73**, 55–63.
13 O. Senol, T. R. Viljava and A. O. I. Krause, *Catal. Today*, 2005, **106**, 186–189.

14 A. Y. Bunch, X. Wang and U. S. Ozkan, *J. Mol. Catal. A: Chem.*, 2007, **270**, 264–272.
15 D. Kubička and J. Horáček, *Appl. Catal., A*, 2011, **394**, 9–17.
16 L. Nie, P. M. de Souza, F. B. Noronha, W. An, T. Sooknoi and D. E. Resasco, *J. Mol. Catal. A: Chem.*, 2014, **388**, 47–55.
17 D. E. Resasco, *J. Phys. Chem. Lett.*, 2011, **2**, 2294–2295.
18 J. H. Sinfelt, *Bimetallic catalysts: discoveries, concepts, and applications*, Wiley, New York, 1983.
19 S. Zafeiratos, S. Piccinin and D. Teschner, *Catal. Sci. Technol.*, 2012, **2**, 1787–1801.
20 S. A. Khromova, A. A. Smirnov, O. A. Bulavchenko, A. A. Saraev, V. V. Kaichev, S. I. Reshetnikov and V. A. Yakovlev, *Appl. Catal., A*, 2014, **470**, 261–270.
21 E. Grootendorst, R. Pestman, R. Koster and V. Ponec, *J. Catal.*, 1994, **148**, 261–269.
22 K. Kandel, J. W. Anderegg, N. C. Nelson, U. Chaudhary and I. I. Slowing, *J. Catal.*, 2014, **314**, 142–148.
23 R. Olcese, M. Bettahar, D. Petitjean, B. Malaman, F. Giovanella and A. Dufour, *Appl. Catal., B*, 2012, **115–116**, 63–73.
24 Y. Ren, M. Yan, J. Wang, Z. C. Zhang and K. Yao, *Angew. Chem., Int. Ed.*, 2013, **52**, 12674–12678.
25 S. Sitthisa, W. An and D. E. Resasco, *J. Catal.*, 2011, **284**, 90–101.
26 S. Leng, X. Wang, X. He, L. Liu, Y. E. Liu, X. Zhong, G. Zhuang and J. G. Wang, *Catal. Commun.*, 2013, **41**, 34–37.
27 T. Kimura, T. Miyazawa, J. Nishikawa, S. Kado, K. Okumura, T. Miyao, N. Shuichi, K. Kimio and K. Tomishige, *Appl. Catal., B*, 2006, **68**, 160–170.
28 B. X. Peng, X. G. Yuan, C. Zhao and J. A. Lercher, *J. Am. Chem. Soc.*, 2012, **134**, 9400–9405.
29 V. M. Gonzalez-DelaCruz, J. P. Holgado, R. Pereñíguez and A. Caballero, *J. Catal.*, 2008, **257**, 307–314.
30 V. A. Yakovlev, S. A. Khromova, O. V. Sherstyuk, V. O. Dundich, D. Yu. Ermakov, V. M. Novopashina, M. Yu. Lebedev, O. Bulavchenko and V. N. Parmon, *Catal. Today*, 2009, **144**, 362–366.
31 T. B. Reed, *Free energy of formation of binary compounds*, MIT press, 1971.
32 R. Pestman, R. Koster, J. Pieterse and V. Ponec, *J. Catal.*, 1997, **168**, 255–264.
33 R. Pestman, R. Koster, E. Boellaard, A. Van der Kraan and V. Ponec, *J. Catal.*, 1998, **174**, 142–152.
34 T. Yokoyama and N. Yamagata, *Appl. Catal., A*, 2001, **221**, 227–239.
35 R. J. Matyi, L. H. Schwartz and J. B. Butt, *Catal. Rev.: Sci. Eng.*, 1987, **29**, 41.
36 J. Ashok and S. Kawi, *ACS Catal.*, 2014, **4**, 89–301.
37 B. Mile, D. Stirling, M. A. Zammitt, A. Lovell and M. Webb, *J. Catal.*, 1988, **114**, 217–229.
38 X. Gao, J. Shen, Y. Hsia and Y. Chen, *J. Chem. Soc., Faraday Trans.*, 1993, **89**, 1079–1084.
39 X. Ge, M. Li and J. Shen, *J. Solid State Chem.*, 2001, **161**, 38–44.
40 E. E. Unmuth, L. H. Schwartz and J. B. Butt, *J. Catal.*, 1980, **61**, 242–255.
41 W. Gao, C. Li, H. Chen, M. Wu, S. He, M. Wei, D. G. Evans and X. Duan, *Green Chem.*, 2014, **16**, 1560–1568.
42 T. Ishihara, K. Eguchi and H. Arai, *Appl. Catal.*, 1987, **30**, 225–238.
43 C. R. F. Lund and J. A. Dumesic, *J. Catal.*, 1981, **72**, 21–30.
44 D. Li, M. Koike, L. Wang, Y. Nakagawa, Y. Xu and K. Tomishige, *ChemSusChem*, 2014, **7**, 510–522.
45 L. Wang, D. Li, M. Koike, S. Koso, Y. Nakagawa, Y. Xu and K. Tomishige, *Appl. Catal., A*, 2011, **392**, 248–255.
46 K. Gheisari, S. Javadpour, J. T. Oh and M. Ghaffari, *J. Alloys Compd.*, 2009, **472**, 416–420.
47 D. Pandey and G. Deo, *J. Mol. Catal. A: Chem.*, 2014, **382**, 23.
48 J. H. Sinfelt, *Acc. Chem. Res.*, 1977, **10**, 15–20.
49 E. K. Parks, K. P. Kerns and S. J. Riley, *Chem. Phys.*, 2000, **262**, 151–167.
50 C. Kittel, *Introduction to Solid State Physics*, Wiley, New York, 5th edn, 1976.
51 T. Mizushima, K. Tohji, Y. Udagawa, M. Harada, M. Ishikawa and A. Ueno, *J. Catal.*, 1988, **112**, 282–289.
52 H. Tanaka, R. Kaino, K. Okumura, T. Kizuka, Y. Nakagawa and K. Tomishige, *Appl. Catal., A*, 2010, **378**, 175–186.
53 L. Guczi, *Catal. Rev.: Sci. Eng.*, 1981, **23**, 329–376.
54 Y. Yang, J. Chen and H. Shi, *Energy Fuels*, 2013, **27**, 3400–3409.
55 J. Chen, H. Shi, L. Li and K. Li, *Appl. Catal., B*, 2014, **144**, 870–884.
56 P. Decyk, M. Trejda, M. Ziolek, J. Kujawa, K. Głaszczka, M. Bettahar, S. Monteverdi and M. Mercy, *J. Catal.*, 2003, **219**, 146–155.
57 G. Connell and J. Dumesic, *J. Catal.*, 1987, **105**, 285–298.
58 C. N. R. Rao, G. U. Kulkarni, K. R. Kannan and S. Chaturvedi, *J. Phys. Chem.*, 1992, **96**, 7379–7385.
59 G. B. Raupp and W. N. Delgass, *J. Catal.*, 1979, **58**, 337–347.
60 W. Rachmady, *J. Catal.*, 2002, **208**, 158–169.
61 W. Rachmady and M. A. Vannice, *J. Catal.*, 2002, **209**, 87–98.
62 C. Dupont, R. Lemeur, A. Daudin and P. Raybaud, *J. Catal.*, 2011, **279**, 276–286.
63 T. Marinelli, S. Nabuurs and V. Ponec, *J. Catal.*, 1995, **151**, 431–438.
64 J. H. Sinfelt, J. L. Carter and D. J. C. Yates, *J. Catal.*, 1972, **24**, 283–296.
65 I. Gandarias, J. Requies, P. L. Arias, U. Armbruster and A. Martin, *J. Catal.*, 2012, **290**, 79–89.

